Ocean Systems Engineering, *Vol. 15, No. 1 (2025) 63-89*
https://doi.org/10.12989/ose.2025.15.1.063

Equivalent plate method for calculating responses of multi-body floating structure with beam connectors

Byoung Wan Kim*

Korea Research Institute of Ships & Ocean Engineering (KRISO), Daejeon, South Korea
University of Science and Technology (UST), Daejeon, South Korea

(Received November 27, 2024, Revised February 26, 2025, Accepted March 8, 2025)

Abstract. This paper proposed an equivalent plate method to simply analyze multiple floating bodies connected with many beam structures. Proposed method assumes a complicated beam grillage structure as a simple plate by introducing equivalent bending thickness and equivalent distributed mass. With this scheme, we can get a approximate but simpler model to reduce Finite Element Method (FEM) computation. A multi-body floating solar platform with 400 floaters, 200 mooring lines and 100 connector beams were analyzed as a numerical example. Added mass, hydrodynamic damping and wave forces of floating bodies were formulated by Higher Order Boundary Element Method (HOBEM) and the elastic equations of beam or plate were formulated by FEM. By solving the combined equation, body motions, mooring lines tensions and section forces such as shear forces, bending moments and torsion moments in regular & irregular waves were obtained. Responses by wind or current were also investigated. All the results by the equivalent proposed method were compared with the original beam grillage analysis results to check efficiency and accuracy of the proposed method.

Keywords: beam connectors; body motion; equivalent plate analysis; FEM; floating solar platform; HOBEM; mooring line tension; multiple floating bodies; section force

1. Introduction

Recently, floating solar platform is tried frequently for alternative energy generator and related studies were done by many researchers. Zheng *et al*. (2021) examined stochastic responses of a floating solar platform combined with wind turbine and aquaculture system. Experimental model test was done by Kim *et al*. (2021) to estimate hydrodynamic performance of a 4-MW floating photovoltaic system with many floaters and beam connectors. Abbasnia *et al*. (2022) studied dynamic responses of a solar platform with twin tubular floaters. Xu and Wellens (2022) analyzed fluid-structure interactions of a large polymer floating solar system in waves. Jiang *et al*. (2023) designed a multi-body floating solar system with soft connection and performed a model test for the system. *Song et al*. (2023) simulated wave induced responses of a floating solar structure with cylinder floaters and steel frame connectors. The floating solar platform generally applies multi-body type to floaters. Hydro-elastic research for multi-body floaters was recently studied by Jin *et al*. (2025). In many cases, engineers apply frame type structure with beam grillage instead of

*Corresponding author, Dr., E-mail: kimbw@kriso.re.kr

http://www.techno-press.org/?journal=ose&subpage=7 ISSN: 2093-6702 (Print), 2093-677X (Online)

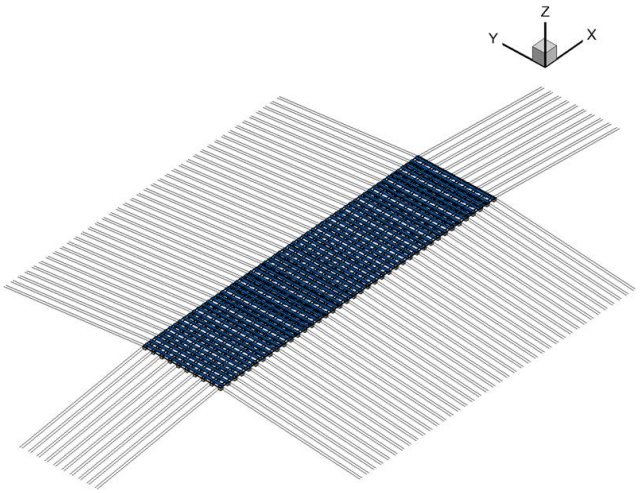

Fig. 1 Geometry of example structure

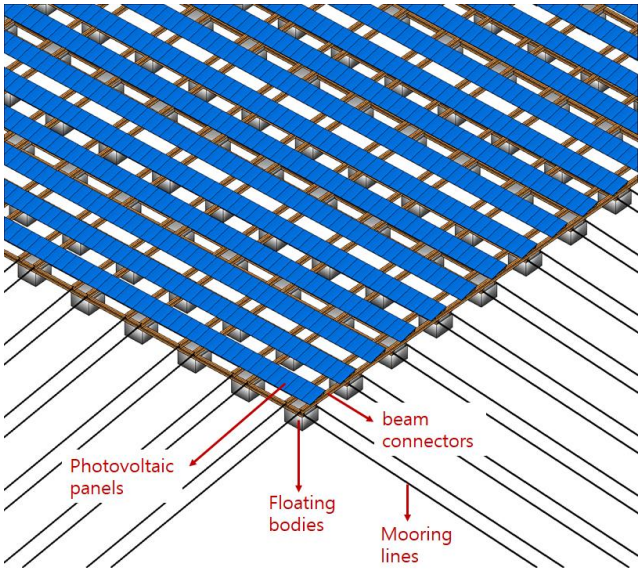

Fig. 2 Detail view of example structure

ship type structure to save cost in building solar platform. The platform usually has many floating bodies and many beam connectors and the structural feasibility were examined by some previous studies (Hong *et al*. 2018, Kim *et al*. 2020, Kim *et al*. 2021, Kim and Lee 2024, Song *et al*. 2023).

Since the beam grillage type platform has many floaters and many beams, its numerical model will be complicated and it needs many efforts to get the FEM model (see Fig. 3). This paper

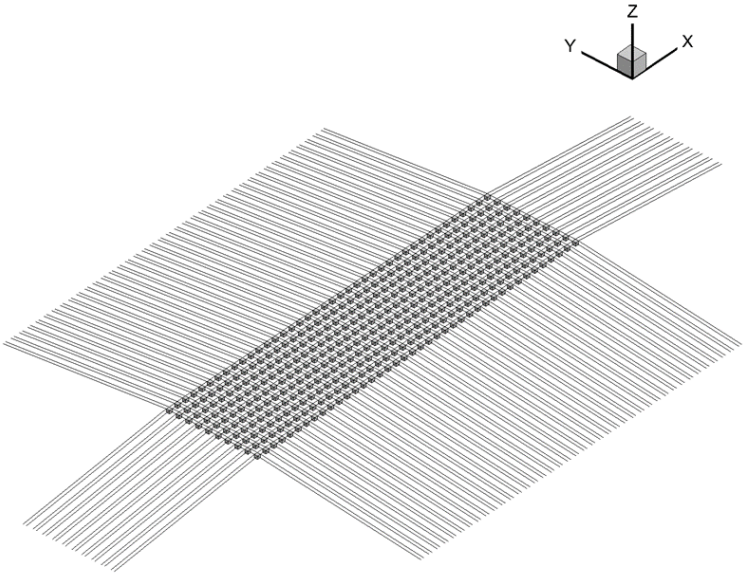

(a) Total view

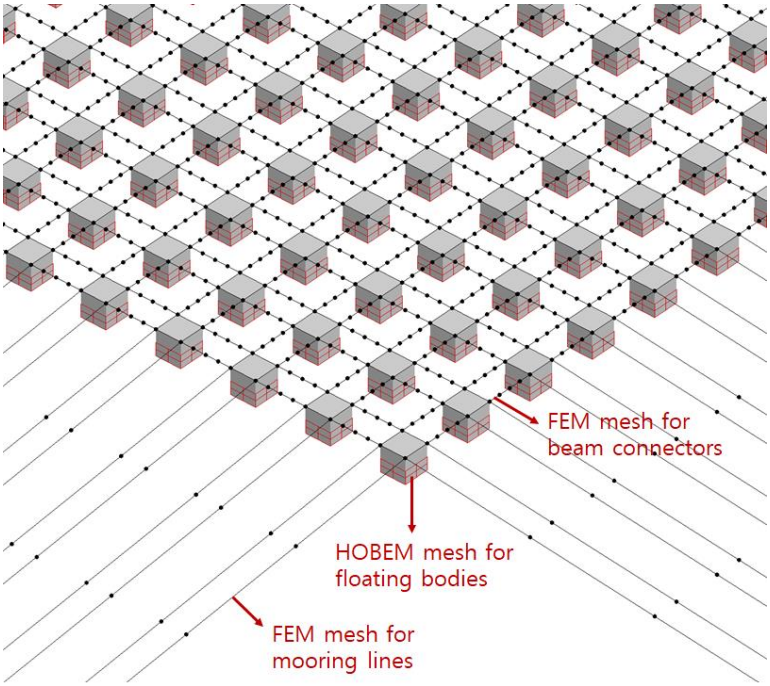

(b) Detail view

Fig. 3 Numerical model of example structure

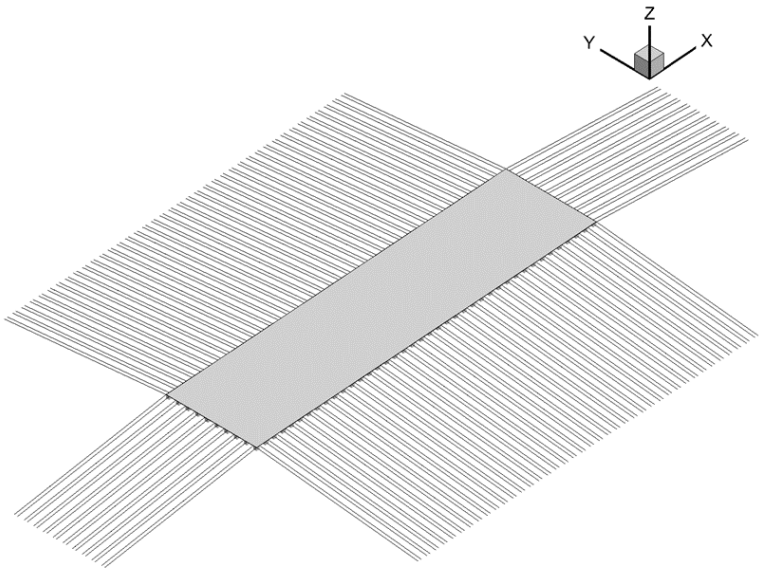

(a) Total view

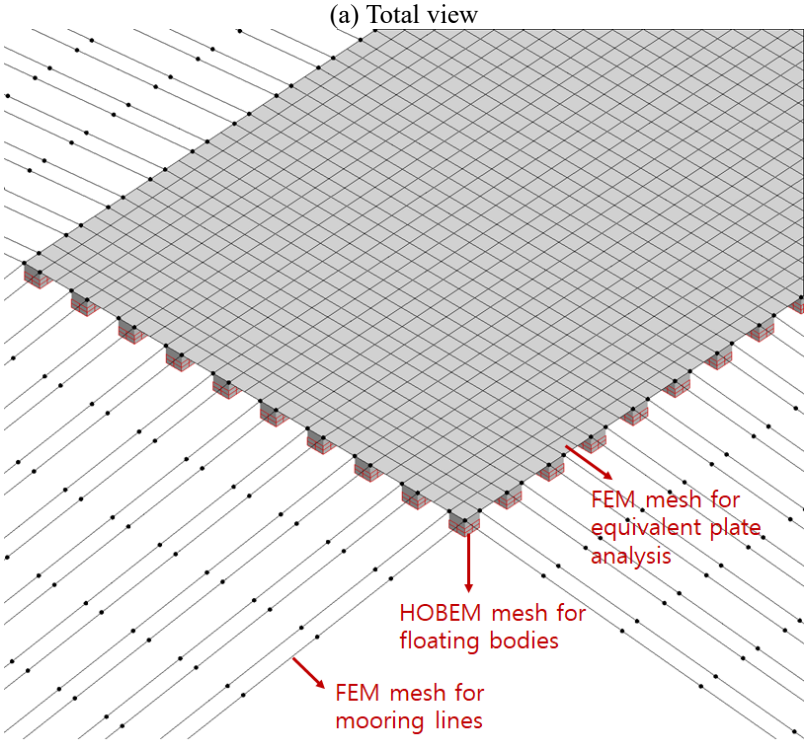

(b) Detail view

Fig. 4 Equivalent plate model for example structure

proposed a equivalent plate method by applying a simple plate for the beam grillage with equivalent bending thickness and mass distribution with assuming that bending mode and behavior of the beam grillage and the equivalent plate are similar. Numerical model of the plate method is simpler and easier and it will reduce efforts in FEM modeling (see Fig. 4).

A multi-body floating solar platform with beam grillage was analyzed as a numerical example to validate the equivalent plate method. The length, breadth and draft of the example structure is 223.988 m, 56 m and 1 m. It has 400 pontoon-type floating bodies and they are connected with 100 beam connectors. 200 pre-tensioned mooring lines are attached to the system to keep position. Hydrodynamic analyses were done for the example structure. In the analysis, added mass, hydrodynamic damping and wave forces were obtained by HOBEM (Choi *et al*. 2001, Hong *et al*. 2005) and the mass matrix and elastic stiffness matrix for beam or plate were derived from FEM. FEM shell formulation for the equivalent plate were obtained by modified Mindlin element with removing shear locking by substitute strain method (Donea and Lamain 1987) and membrane element with including drilling degree of freedom (Allman 1988). By solving the combined equation for the floaters and beam connectors or plate, dynamic responses such as body motions, mooring line tensions, sectional forces (shear forces, bending moments and torsion moments) in regular & irregular waves were calculated and their results were compared for the original beam grillage analysis and the equivalent plate analysis. Responses by wind or current were also compared. From the numerical results, modeling easiness, computation reduction and numerical accuracy of the equivalent plate method were discussed.

2. Hydrodynamic analysis of multiple floating bodies with beam connectors

Hydrodynamic forces at multi-bodies can be calculated by various numerical methods. Among them, this paper applied HOBEM (Choi *et al*. 2001, Hong *et al*. 2005). HOBEM employs linear velocity potential theory to calculate 1st order wave forces at floating bodies. The potential ϕ has three components.

$$\phi = \phi_I + \phi_S + \phi_R \tag{1}$$

Where, ϕ_I is incident potential by incoming waves, ϕ_S is scattering potential by reflected or transmitted waves at body surfaces and ϕ_R is radiation potential by radiated waves from body motions. $\phi_D = \phi_I + \phi_S$ is diffraction potential. Analytic solutions for ϕ_I are generally known but analytic calculation for ϕ_S and ϕ_R is very hard. So, numerical schemes such as HOBEM are generally applied. The procedures are summarized. Governing equation for scattering potential takes the following Laplace form as (2) and the boundary conditions are (3)~(6).

$$\nabla^2 \phi_S = 0 \qquad \text{at sea domain} \tag{2}$$

$$\frac{\partial \phi_S}{\partial z} = \frac{\omega^2}{g} \qquad \text{at free surface of water plane} \tag{3}$$

$$\frac{\partial \phi_S}{\partial n} = 0 \qquad \text{at sea bottom} \tag{4}$$

$$\lim_{r \to \infty} \sqrt{r} \left(\frac{\partial \phi_S}{\partial r} - ik\phi_S \right) = 0 \qquad \text{at infinite radial boundary} \tag{5}$$

$$\frac{\partial \phi_S}{\partial n} = -\frac{\partial \phi_I}{\partial n} \qquad \text{at bodies surfaces} \tag{6}$$

Where, $\nabla^2 = \frac{\partial^2}{\partial x^2} + \frac{\partial^2}{\partial y^2} + \frac{\partial^2}{\partial z^2}$, ω is angular frequency of wave, g is acceleration of gravity, $i = \sqrt{-1}$, k is wave number, $\frac{\partial}{\partial n} = \vec{n} \cdot \nabla$, $\vec{n}$ is normal vector at body surface, $\nabla = \left(\frac{\partial}{\partial x}, \frac{\partial}{\partial y}, \frac{\partial}{\partial z}\right)$. HOBEM applies free-surface Green function which satisfies (2)~(5) and sets up numerical grids for body surface boundary elements with 9-node higher order interpolation to solve (6). Finally, it formulates the following discrete algebraic boundary integral equations.

$$[H]\{\phi_S\} = -[G]\left\{\frac{\partial \phi_I}{\partial n}\right\} \tag{7}$$

Where, [G] is matrix of Green functions, [H] is matrix of Green function derivatives. Radiation potential is calculated in the similar way. Its governing equation and boundary conditions at free surface, sea bottom and infinite radial boundary have the same form as (2)~(5). Boundary condition at body surface of radiation potential is

$$\frac{\partial \phi_R}{\partial n} = -i\omega u_n \qquad \text{at bodies surfaces} \tag{8}$$

Where, $u_n = \vec{n} \cdot \vec{u}$ and $\vec{u}$ is vector of mode shape of floating body. Its discrete algebraic equation can be derived by the similar way in scattering potential. It takes the form.

$$[H]\{\phi_R\} = -i\omega[G]\{u_n\} \tag{9}$$

From the solutions of (7) and (9), pressure can be calculated by Bernoulli equation as

$$p = i\omega\rho(\phi_I + \phi_S + \phi_R) - \rho g u_z \tag{10}$$

where p is pressure at body surface, ρ is water density, u_z is vertical motion at body surface. In this study, pressure in the floating body by waves were calculated by linearization at mean body position. So, the Eq. (10) takes the linear form. By integrating (10), wave forces at floating bodies are calculated and the the following equation of motion for floating bodies are derived.

$$[M_B + M_{add}]\{\ddot{u}_B(t)\} + [C_B]\{\dot{u}_B(t)\} + [K_B]\{u_B(t)\} = \{f_{wave}(t)\} \tag{11}$$

Where, [M_B] is mass matrix of floating bodies. [K_B] is matrix of restoring force coefficients and they are derived from the part of u_z in (10). [M_{add}] and [C_B] are added mass matrix and hydrodynamic damping matrix, respectively. They are derived from the part of radiation potential ϕ_R in (10). {u_B} is vector of floating body motions. The matrix order will be $6N_B \times 6N_B$ and vector order will be $6N_B$ if number of bodies is N_B because each body has six degrees of freedom (dof) such as surge, sway, heave, roll, pitch and yaw at its center. {$f_{wave}(t)$} is time domain wave force vector and it can be obtained by the following time domain conversion of the frequency domain wave forces.

$$f_{wave}(t)\begin{cases} = Re\left\{\frac{H}{2} f_{wave}(\omega) e^{-i\omega t}\right\} & \text{(Regular)} \\ = \sum_{j=1}^{N_\omega} Re\left\{\sqrt{2S(\omega_j)\Delta\omega} f_{wave}(\omega_j) e^{-i(\omega_j t + \psi_j)}\right\} & \text{(Irregular)} \end{cases} \tag{12}$$

where H is wave height and $f_{wave}(\omega)$ is Response Amplitude Operator (RAO) of wave forces in frequency domain. $f_{wave}(\omega)$ is complex value and they are derived from the part of diffraction potential $\phi_D = \phi_I + \phi_S$ in (10). $S(\omega)$ is design wave spectrum (ex: JONSWAP spectrum) and it is function of H_s (significant wave height), T_p (peak period) and γ (shape parameter). $\Delta\omega$ is frequency step, ψ is random phase angle, N_ω is number of frequency points. In this way, floating bodies with any geometry can be analyzed with the HOBEM and body-to-body interactive diffraction forces of multi-bodies are calculated. Interactive radiation forces are also calculated by HOBEM and entire coupled effects of radiation of multi-bodies can be simulated if mode shapes of each body are employed as boundary conditions. More details of HOBEM can be found in the previous studies (Choi *et al*. 2001, Hong *et al*. 2005).

Time domain equation of motion for beam connectors and mooring lines takes the following form.

$$[M]\{\ddot{u}(t)\} + [C]\{\dot{u}(t)\} + [K]\{u(t)\} = \{f_{wm}(t)\} \tag{13}$$

where $[M]$ is mass matrix of beam connectors and mooring lines, $[K]$ is elastic stiffness matrix. They can be formulated by FEM and detailed process for beams and mooring lines are shown in some previous studies (Kim *et al*. 1999, Garret 2005, Kim *et al*. 2013, Kim *et al*. 2019). $[C]$ is damping matrix and linear combination of $[M]$ and $[K]$ such as Rayleigh damping is usually used. $\{u\}$ is motion vector of beams and mooring lines. $\{f_{wm}(t)\}$ is wave force vector at mooring lines. In this study, Morison equation is used to calculate wave forces at mooring lines because the mooring lines are slender. Matrix order will be $N \times N$ and vector order will be N if total dof is N. N is determined from nodal points and boundary conditions in FEM model.

Time domain equation of motion for total system with floating bodies, beam connectors and mooring lines is derived by combining (11) and (13).

$$[M + M_B + M_{add}]\{\ddot{u}(t)\} + [C + C_B]\{\dot{u}(t)\} + [K + K_B]\{u(t)\} = \{f_{wave}(t) + f_{wm}(t)\} \tag{14}$$

This study set up common nodal points at floating body centers and they were connected to body-beam bolting points with rigid link elements. In this way, terms of mass, damping, restoring force coefficients and wave forces of floating bodies can be connected to corresponding parts of (13) because $u_B = u$ at common nodes. 2nd order drift forces by waves, wind forces or current forces other than 1st order wave forces can be included by adding them to the right side of (14). In this study, drift forces were also calculated by HOBEM (Choi *et al*. 2001). Wind and current forces were calculated in Morison form. Time domain solution of (14) can be obtained by many time marching methods and this study applied Newmark method (Newmark 1959, Chung and Hulbert 1993) to solve (14). From the solution, dynamic responses such as body motions, mooring line tensions, sectional shear forces, bending moments and torsion moments are obtained.

3. Equivalent plate analysis

Equivalent plate method assumes that the bending mode and behavior of beam grillage is similar to those of a plate if the equivalent bending stiffness and mass distribution are found. The equivalent bending thickness of the equivalent plate can be derived by matching total bending stiffness of original beam section and plate section as

$$N_x I = \frac{B t_{equiv}^3}{12} \tag{15}$$

where N_x is number of beams in longitudinal direction, I is second moment of area of beam section, B is breadth of total structure, t_{equiv} is equivalent bending thickness. Then, equivalent thickness is derived as

$$t_{equiv} = \left(\frac{12 N_x I}{B}\right)^{1/3} \tag{16}$$

Distributed mass of the equivalent plate can be obtained by matching total beam mass as

$$m(N_x L_x + N_y L_y) = \mu B L \tag{17}$$

where m is mass per length of beam, L_x is length of longitudinal beam, N_y is number of beams in lateral direction, L_y is length of lateral beam, μ is equivalent distributed mass per area of plate, L is length of total structure. Then, equivalent distributed mass per area is derived as

$$\mu = \frac{m(N_x L_x + N_y L_y)}{BL} \tag{18}$$

In the equivalent plate analysis, [M], [C] and [K] of the beam grillage in (14) are replaced by those of equivalent plate. Stiffness and mass matrices of the plate model can be derived from FEM shell formulation. Elastic stiffness matrix of shell, [K] is derived by assembling stiffness matrix of each shell element.

$$[K] = \sum_{element} \begin{bmatrix} [K_{plate}] & [0] \\ [0] & [K_{membrane}] \end{bmatrix} \tag{19}$$

Shell element has two parts. One is plate part and the other is membrane part. Plate part describes bending, torsion and vertical shear behaviors of shell and [K_{plate}] in (19) is the plate element stiffness matrix. It takes the form.

$$[K_{plate}] = \int_V [B_p]^T [D_p][B_p] dV \tag{20}$$

Where, [B_p] is strain-displacement relation matrix and [D_p] is elasticity matrix for vertical displacement and rotational displacement about x or y axis. $\int_V dV$ represents volumetric integration. This study applied Mindlin element because it can simulate thick shell as well as thin shell. Conventional Mindlin element over-estimates shear stiffness in a thin shell. This study employed modified Mindlin element with substitute strain field method to remove the shear locking. More details for (20) with substitute strain method are shown in the study by Donea and Lamain (1987). [$K_{membrane}$] in (19) is stiffness matrix for membrane behavior and it describes tension, compression and lateral shear behaviors. It takes the form.

$$[K_{membrane}] = \int_V [B_m]^T [D_m][B_m] dV \tag{21}$$

Where, [B_m] is strain-displacement relation matrix and [D_m] is elasticity matrix for lateral displacements. This study applied the membrane element with including drilling dof (rotational displacement about z axis) for (21). The detail form of (21) with including drilling dof are found in the study by Allman (1988). Mass matrix, [M] is obtained by assembling element mass matrix [$M_{element}$] as

$$[M] = \sum_{element}[M_{element}] \tag{22}$$

$$[M_{element}] = \int_V \mu[N]^T[N]dV \tag{23}$$

where μ is mass per area, [*N*] is matrix of shape functions which define the relation between internal displacements and nodal displacements in a shell element. The formulation details are found in many text books of FEM. Then, damping matrix, [*C*] can be obtained by linear combination of [*M*] and [*K*] such as Rayleigh damping. By replacing these [*M*], [*C*] and [*K*] to (14), hydrodynamic analysis with shell can be performed.

4. Numerical analysis for example structure

A multi-body system with beams and mooring lines were analyzed as a numerical example to verify the equivalent plate method. The sample structure is a floating solar platform supporting photovoltaic panels as Figs. 1 and 2. Proposed equivalent plate method can be applied to multi-body floating structures with many beam connectors. And, floating offshore solar platform was considered as a numerical example because it is the typical type of the multi-body floating system with many beam connectors. Main properties of the example structure is based on the design sample by KRISO (2020~2024). Length and breadth of the system are 223.988 m and 56 m. It has 56 arrays of photovoltaic panels row and each row has 58 panels. So, total number of panels is 56×58=3248. Electric power of each panel is 400 W. Therefore total power is 400×3248=1.3 MW. Total length of the example structure is 223.988 m and the breadth is 56 m. Draft is 1 m and the total mass is 1,600 ton. It has 400 pontoon floaters and they are connected with 100 beam connectors. The connector is aluminum I-beam. Beams are connected with pontoons by bolting connection. 200 mooring lines are attached to the system. Pre-tensioned polyester ropes are used for the mooring lines. The diameter of mooring line is 44 mm and its MBF (minimum breaking force) is 252 kN. The geometry and numerical model are shown in Figs. 1-3. The material properties of floaters, beams and mooring lines are summarized in Table 1. In the table, x_L is horizontal distance from anchor to fairlead of mooring line, z_L is vertical distance, s_L is total length. C_D, C_M, C_F, C_a are drag, mass, friction, added mass coefficients of mooring lines. Design values for wave, wind and current are also summarized in Table 1. Target site of the sample structure is Saemangeum area in Gunsan in South Korea. Significant height of design wave is 1.5 m and the peak period is 9 s. Design current speed is 0.319 m/s. They are determined from the results of environmental assessment for the site. Design wind speed is 55 m/s and the value is determined from the Korean design standard (Korea Ministry of Oceans and Fisheries 2017). Design conditions of wave, wind and current were determined separately and extreme values in each case were chosen focusing on safe design.

Design wind speed is very high (55 m/s) in the site and mooring line tension by wind is big (47.932 kN) as show in Table 6. Tension by current is 2.017 kN (see Table 6). Maximum tension in waves is 9.66 kN (see Table 5). Pretension is 48.973 kN (see Table 1). Therefore, total tension is 108.582 kN and the safety factor about MBF is 252/108.582=2.3. 200 mooring lines were chosen in such way that safety factor of the total calculated tension is bigger than 2. So, many mooring lines were attached to endure wind & current forces as well as wave forces. Layout of many mooring lines were also shown in other researches (Kim *et al*. 2021, Kim and Lee 2024).

Table 1 Material properties and wave conditions of example structure

Total structure	Type		1.3 MW floating solar platform
	Water depth		10 m
	Length(L)×Breadth(B)×Draft(d)		223.988×56×1 m
	Mass	Floating bodies	800,000 kg
		Beams grillage	800,000 kg
		Total	1,600,000 kg
	Distance from bottom to gravity center (KG)		1 m
Floating body	Type		Pontoon
	No. of bodies		400
	Length×Breadth×Height×Draft of 1 body		2×2×2×1 m
Mooring line	Type		Polyester rope (D=44 mm, MBF=252 kN)
	No. of lines		200
	Axial stiffness (EA)		1.845×10^9 N
	Pre-tension (T_0)		48.973 kN
	Mass per length (m)		1.47 kg/m
	$x_L/z_L/s_L$		100/11/100.603 m
	$C_D/C_M/C_F/C_a$		1.2/2.0/0.05/1.0
Beam	Type		Al I-beam
	No. of beams	Longitudinal (N_x)	20
		Lateral (N_y)	80
		Total	100
	Beam length	Longitudinal length (L_x)	223.988 m
		Lateral length (L_y)	56 m
	Breadth×Height×Thickness of beam section		340×380×30 mm
	Young's modulus (E)		6.96×10^{10} Pa
	Bending stiffness (EI)		49,290,720 N-m^2
	Torsion stiffness (GJ)		235,489 N-m^2
	Mass per length (m)		89.288 kg/m
Wave	Regular waves for RAO analysis	Height (H)	2 m
		Period (T)	3~45 s
		Heading angle (β)	0, 45, 90 deg
	Irregular wave for design condition	Sig. height (H_s)	1.5 m
		Peak period (T_p)	9 s
		Shape parameter (γ)	2.5
		Heading angle (β)	0, 45, 90 deg
Wind	Wind speed		55 m/s
	Direction (β)		180 deg
	C_D of topside above water-line		2.3
Current	Current speed		0.319 m/s
	Direction (β)		0 deg
	C_D of floater below water-line		2.0

Table 2 Material properties of equivalent plate model

Item	Values
Equivalent bending thickness (t_{equiv})	0.145 m
Equivalent mass per area (μ)	63.779 kg/m^2

Table 3 Natural frequencies and natural periods of example structure

Mode	Natural frequency, f_n (Natural period, T_n)		Error
	Beam grillage analysis	Equivalent plate analysis	
Surge	0.14138 Hz (7.07311 s)	0.14141 Hz (7.07174 s)	0.02%
Sway	0.27364 Hz (3.65443 s)	0.27378 Hz (3.65253 s)	0.05%
Bending	0.38104 Hz (2.62438 s)	0.38026 Hz (2.62981 s)	-0.21%
Torsion	0.39610 Hz (2.52462 s)	0.40239 Hz (2.48514 s)	1.59%

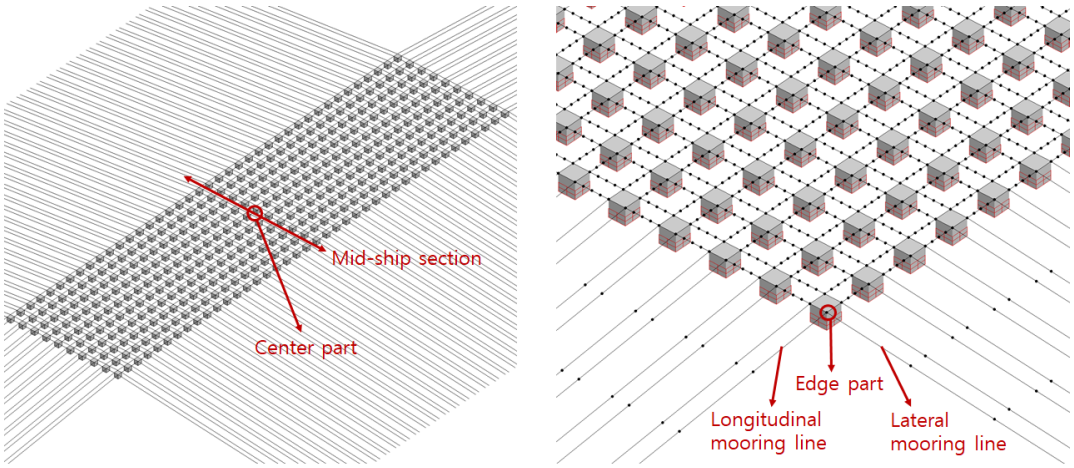

Fig. 5 Location of parts to investigate responses

Responses were investigated for regular & irregular waves, wind and current. In waves, 2nd order drift force are included along with 1st order forces in the simulation. The RAO responses were observed in regular waves for periods are 3~45 s with wave height 2 m. Responses in design irregular waves were also observed. The significant height is 1.5 m and peak period is 9 s. Heading angles of waves (β) are 0, 45, 90 degs. Wind induced responses were observed for design speed 55 m/s. The wind direction is assumed 180 deg because wind force is the biggest when the wind blows behind the photovoltaic panels. Current induced responses were investigated with design speed 0.319 m/s. Mooring tension by current is maximum at β=0 or 180 deg.

Fig. 4 shows the equivalent plate model for the example structure. Equivalent bending thickness and mass per area were calculated by Eqs. (4) and (6) and the results are summarized in

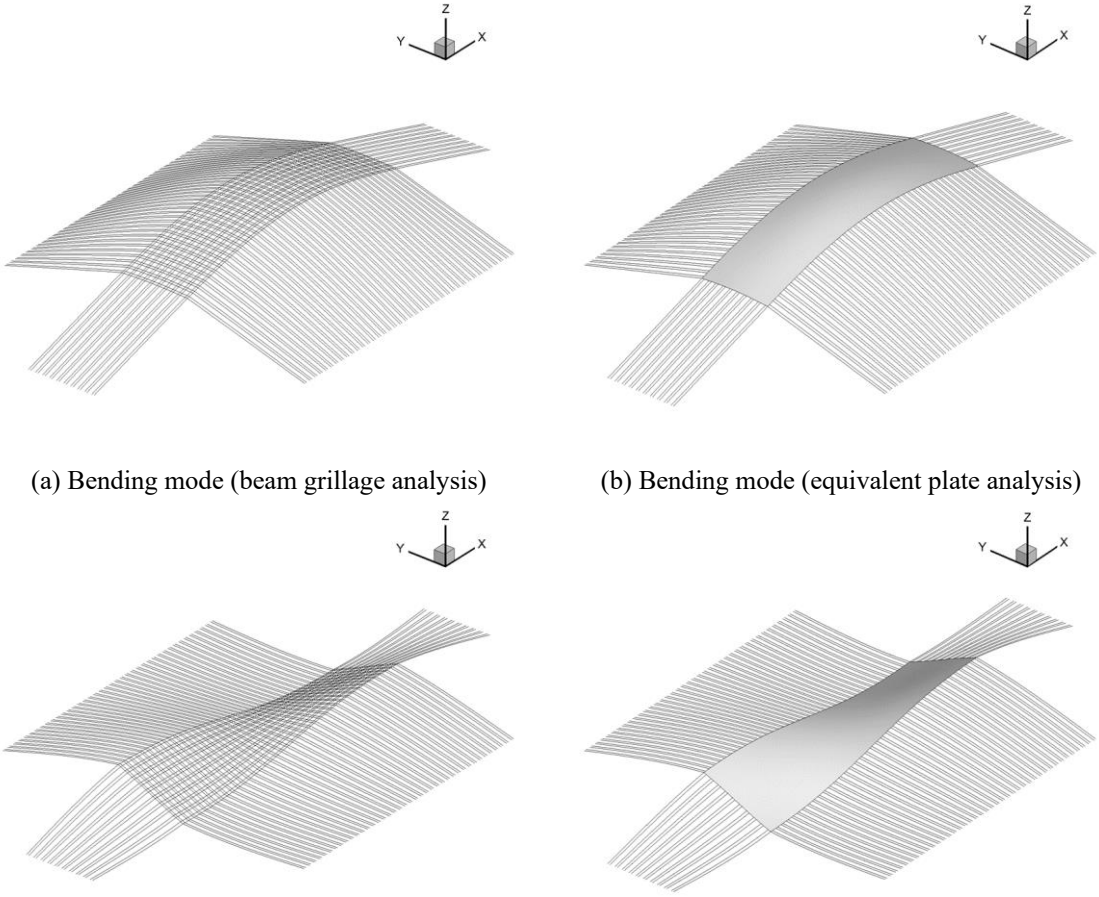

(a) Bending mode (beam grillage analysis) (b) Bending mode (equivalent plate analysis)

(c) Torsion mode (beam grillage analysis) (d) Torsion mode (equivalent plate analysis)

Fig. 6 Mode shapes of the example structure

Table 2. Body motions at center & edge parts, dynamic tension of mooring lines in longitudinal & lateral directions, shear forces & bending moments & torsion moments at mid-ship sections of the equivalent plate model were calculated and the results were compared with the original beam grillage analysis (see Fig. 5 for location of parts to see responses). From the numerical comparisons, modeling efficiency and accuracy of the equivalent plate method were discussed.

Fig. 6 and Table 3 summarize mode shapes and natural frequencies of the example structure. Natural frequencies and mode shapes were calculated by solving the eigenvalue problem.

$$[K + K_B]\{U\} = \omega_n^2[M + M_B + M_{add}]\{U\} \tag{24}$$

where ω_n is natural frequency in rad/s. Then, natural frequency in Hz is $f_n=\omega_n/2\pi$ and natural period is $T_n=1/f_n$. $\{U\}$ is vector of mode shape. This study applied subspace iteration method (Bathe and Wilson 1972, Kim *et al*. 2005) for eigenvalue analysis. It is shown that elastic modes of

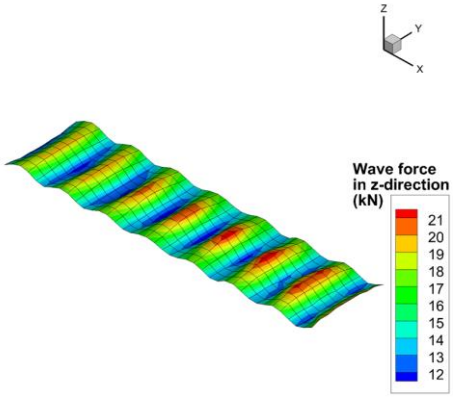

(a) *H*=2 m, *T*=3 s, Heading=0 deg

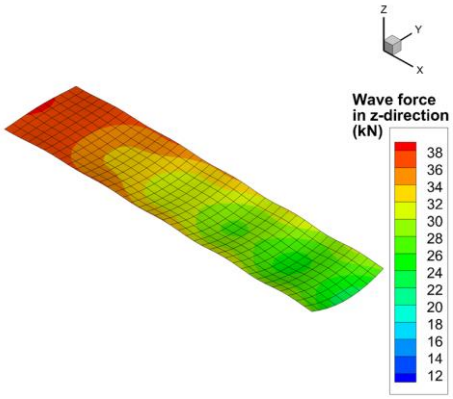

(b) *H*=2 m, *T*=9 s, Heading=0 deg

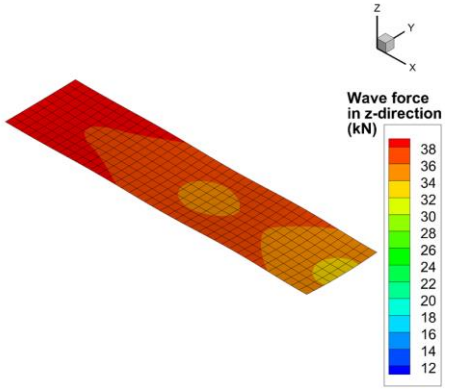

(c) *H*=2 m, *T*=20 s, Heading=0 deg

Fig. 7 Distribution of vertical wave forces at floating bodies of example structure

the beam grillage and equivalent plate analyses are generally similar and especially bending modes are nearly identical. Torsion modes shows some error because the equivalent plate method focused on matching bending stiffness & mass. So, the method will include errors in torsion stiffness and rotational mass.

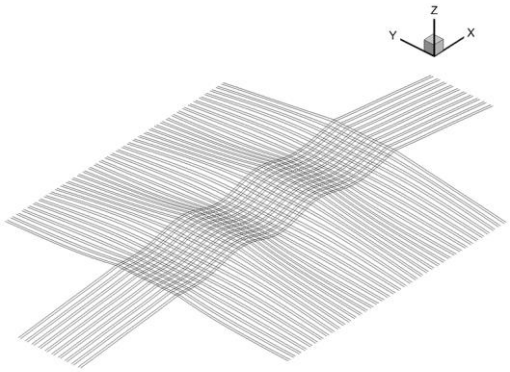

(a) Heading=0 deg (beam grillage analysis)

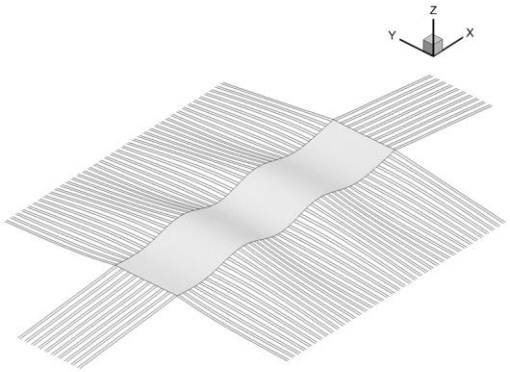

(b) Heading=0 deg (equivalent plate analysis)

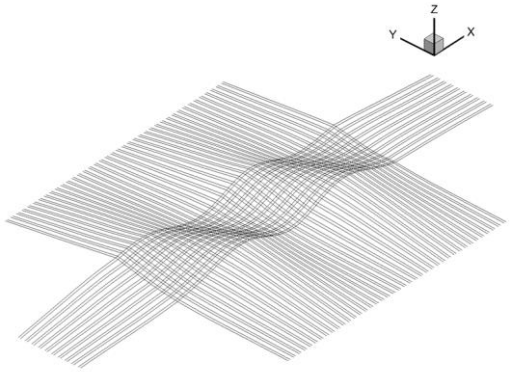

(c) Heading=45 deg (beam grillage analysis)

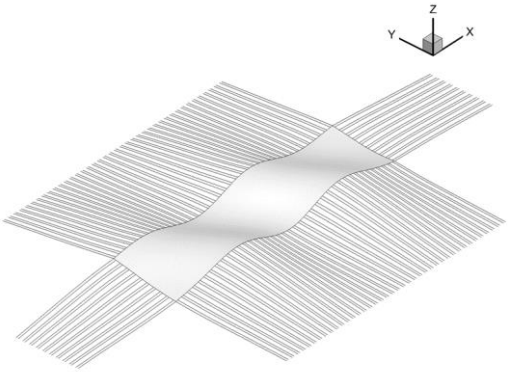

(d) Heading=45 deg (equivalent plate analysis)

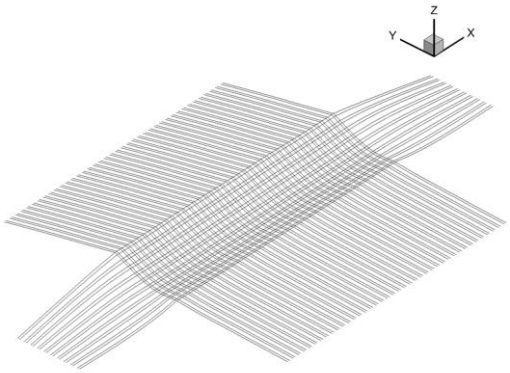

(e) Heading=90 deg (beam grillage analysis)

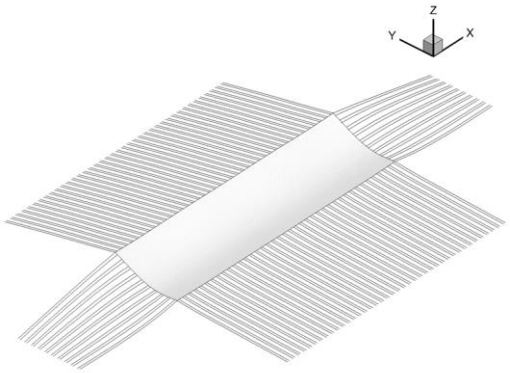

(f) Heading=90 deg (equivalent plate analysis)

Fig. 8 Deformation shape of example structure at t=200 sec (*H*=2 m, *T*=9 s, deformation scale=10)

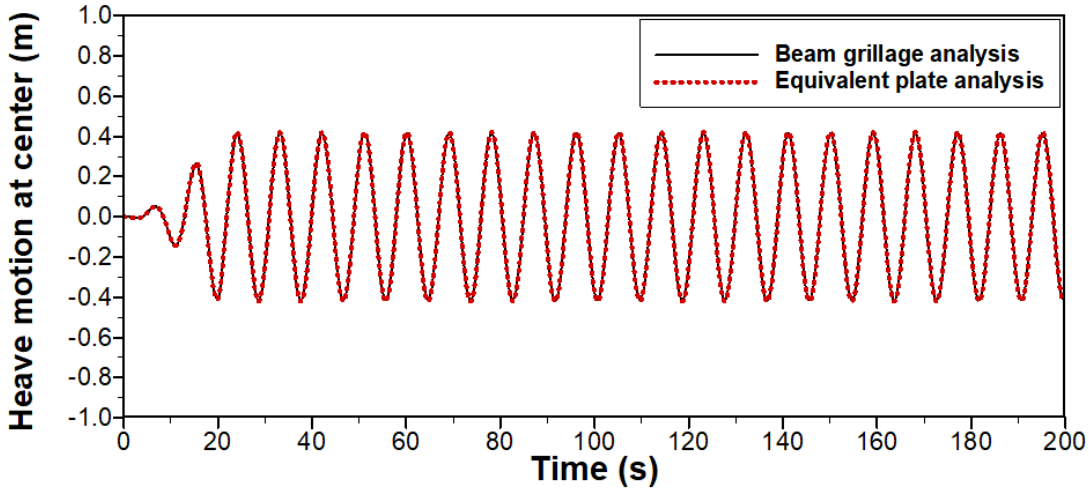

(a) Center point

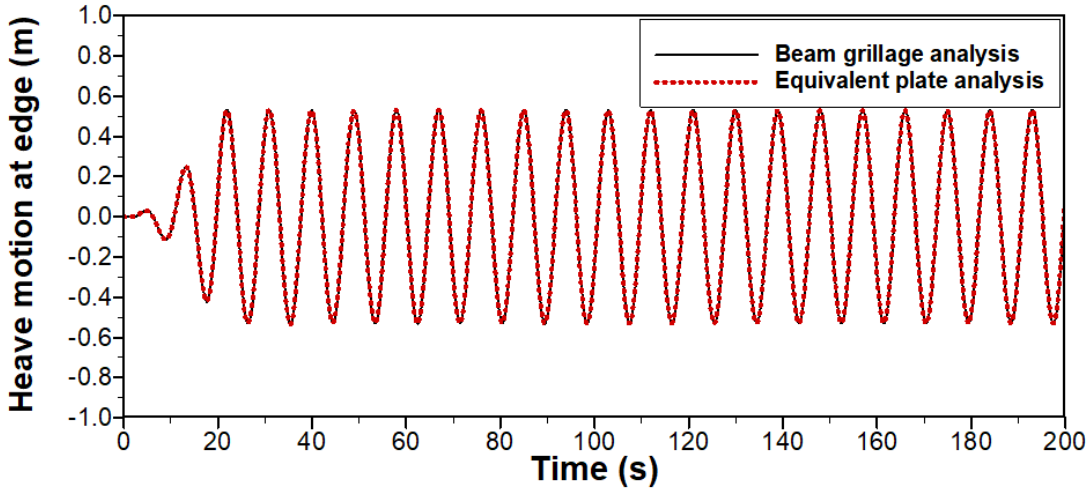

(b) Edge point

Fig. 9 Time series of heave motion at specified points of Fig. 7

In the sample structure, Rayleigh damping matrix is applied for structural damping as (25).

$$[C] = \alpha[M] + \beta[K] \tag{25}$$

with

$$\alpha = \frac{2\xi\omega_1\omega_2}{\omega_1+\omega_2} \tag{26}$$

$$\beta = \frac{2\xi}{\omega_1+\omega_2} \tag{27}$$

where ξ is material damping ratio and ξ=0.02 is assumed in this study. ω_1 and ω_2 are natural frequencies which contribute significantly to dynamic responses. In this structure, lateral tension is

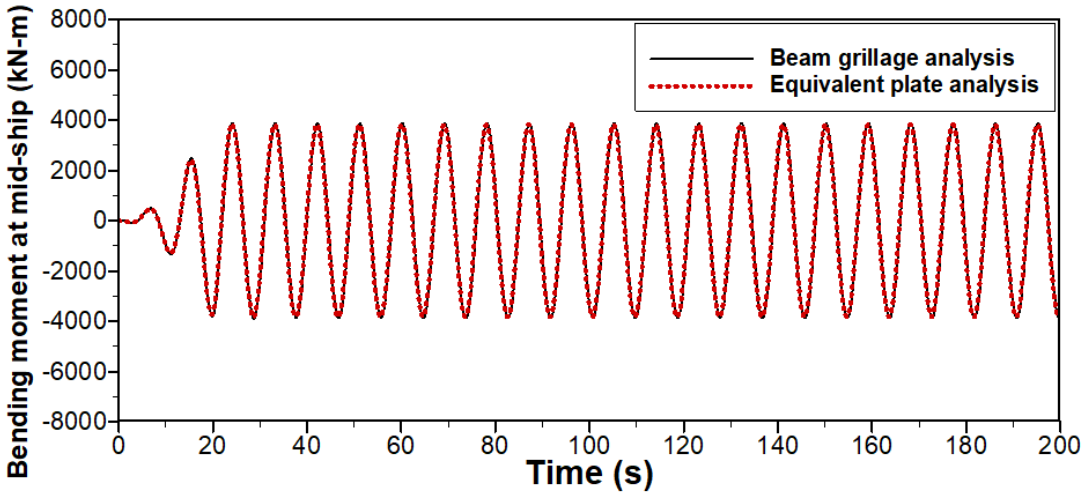

Fig. 10 Time series of bending moment at mid-ship section of example structure in regular waves (H=2 m, T=9 s, heading angle=0 deg)

critical because wave forces are larger in sway direction. So, $\omega_1=\omega_2=\omega_{n,surge}$ = 1.57 rad/s were applied. Then, α=0.0314 and β=0.0127.

Analyses results in regular waves are shown in Figs. 7-16. Fig. 7 shows distribution of wave forces at floating bodies of example structure. In short period, the changes of wave forces between neighboring bodies are noticeable. In longer periods, the changes are small. Fig. 8 shows some snapshot of deformation shape of example structure and its time series of heave motion at certain points are shown in Fig. 9. It is shown that deformation shapes of beam grillage analysis and equivalent plate analysis are nearly equal. Fig. 10 is a sample of time series of responses in regular waves. 200 seconds were simulated for regular cases. By analyzing the signal of time series, RAO can be obtained by.

$$RAO = \frac{y_a}{A} \tag{28}$$

where y_a is amplitude of responses, $A=H/2$ is wave amplitude and H is wave height. The RAO analyses in regular waves were done for wave periods T=3~45 s (wave frequencies ω=2.1~0.14 rad/s) in order to cover the frequency range of the example structure's design spectrum shown in Fig. 11. Figs. 12-16 are the results and RAO of equivalent plate analysis are compared with that of beam grillage analysis. Surge and sway RAO of equivalent plate analysis are very similar to that of beam grillage analysis. Surge has a resonant peak near T=7 s and resonant peak of sway is about T=3.5 s. This result is consistent with Table 3. Heave motions of the two methods are also similar. Mooring line tensions of the two methods are also similar. Longitudinal tension has resonant peak near T=7 s and lateral tension has resonant peak near T=3.5 s. These are associated with surge and sway results because tension is largely affected by surge or sway motion. Shear forces in z-direction and bending moments about y-axis at mid-ship section of the two methods agree well. In case of torsion moment about x-axis in heading angle 45 deg, equivalent plate analysis is similar to beam grillage analysis when wave periods are small. But, it shows some error in large periods.

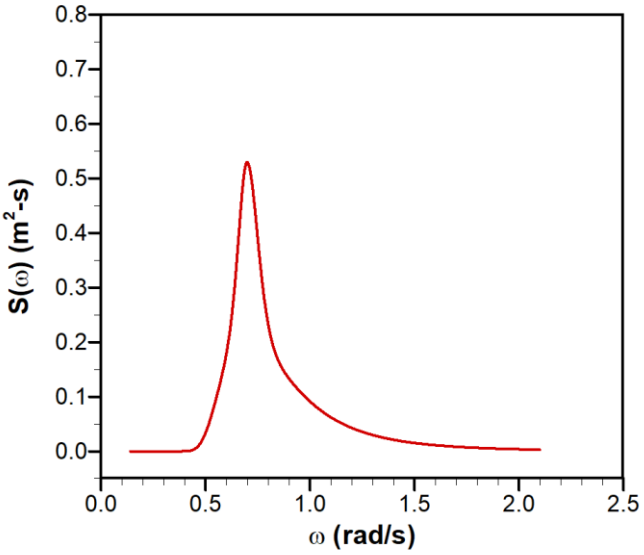

Fig. 11 Design wave spectrum in example structure (H_s=1.5 m, T_p=9 s, γ=2.5, JONSWAP type)

The proposed equivalent plate method focused on matching bending stiffness & mass. Simultaneous matching for bending & torsion stiffness or mass & rotational mass is practically difficult. So, the torsion errors are inevitable. This needs improvement.

Analysis results in irregular waves are summarized in Figs. 17-22. Fig. 17 shows a sample of time series of responses in irregular waves. 3-hour (10,800 seconds) simulations were done for irregular cases. By analyzing the signal of time series, the statistical values in irregular waves can be obtained by

$$Max = \max(|y|) \tag{26}$$

$$Avg = \text{mean}(y_H)/2 \tag{27}$$

where *Max* is maximum response, y is response, *Avg* is average response, y_H is heights of responses by zero-upcrossing. The results for *Max* and *Avg* in irregular waves are summarized in Figs. 18-22 and Tables 4 and 5. It is shown that *Max* or *Avg* for body motions, mooring line tensions, shear forces and bending moments of equivalent plate method agree well to those of the original beam grillage analysis. For peak values, the errors are less than 2%. In torsion moment, errors are bigger and they are 11~12% for peak values. The proposed equivalent plate method focused on matching bending stiffness & mass. Simultaneous matching for bending & torsion stiffness or mass & rotational mass is practically difficult. So, the torsion errors are inevitable. This needs improvement.

Analyses results in winds or currents are summarized in Figs. 23 and 24 and Table 6. Lateral displacements of the platform and tensions of mooring line are compared for beam grillage and equivalent plate analyses. Results of two methods are nearly equal and the numerical errors are less than 1%.

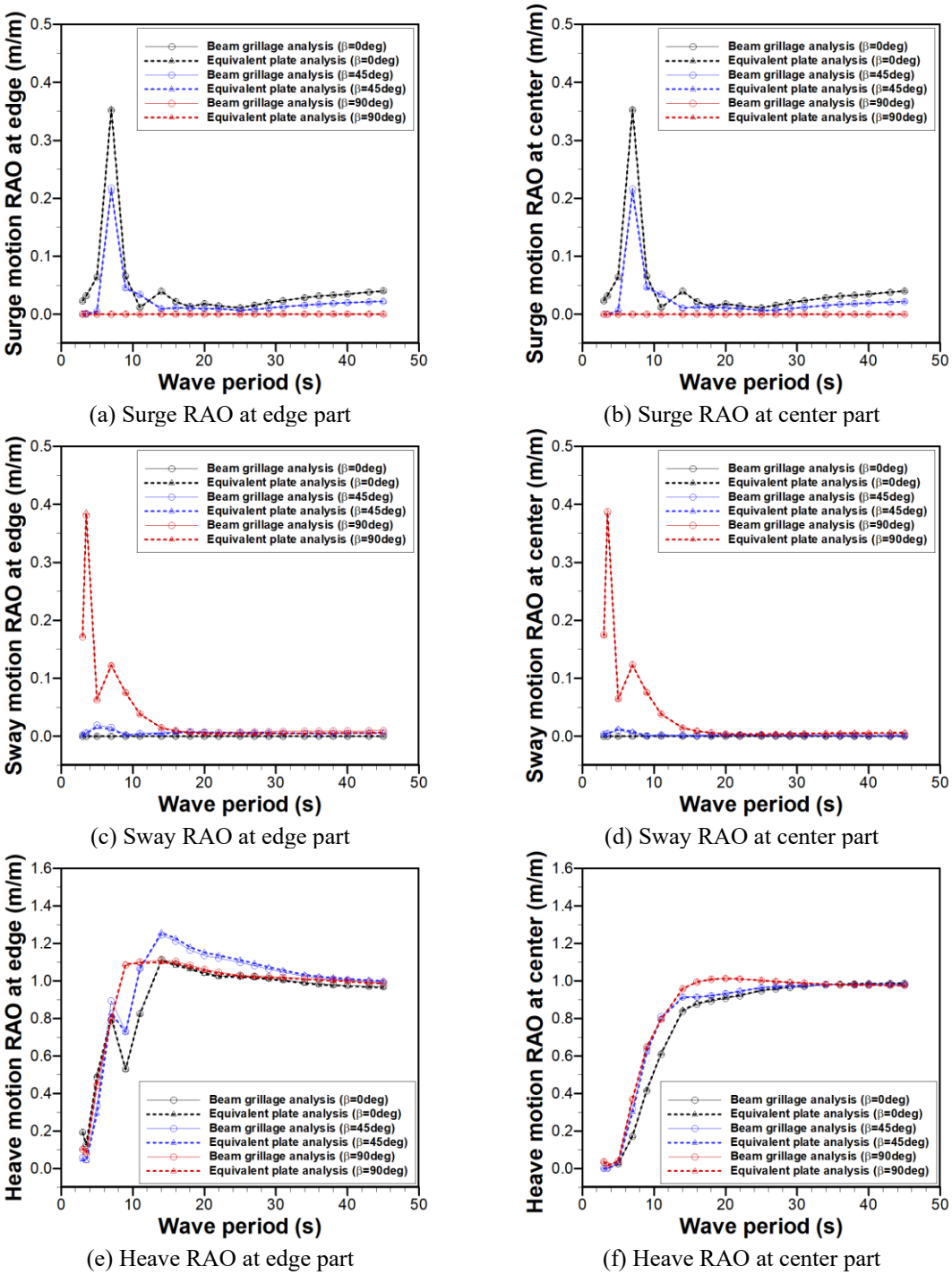

(a) Surge RAO at edge part

(b) Surge RAO at center part

(c) Sway RAO at edge part

(d) Sway RAO at center part

(e) Heave RAO at edge part

(f) Heave RAO at center part

Fig. 12 Motion RAO of example structure in regular waves

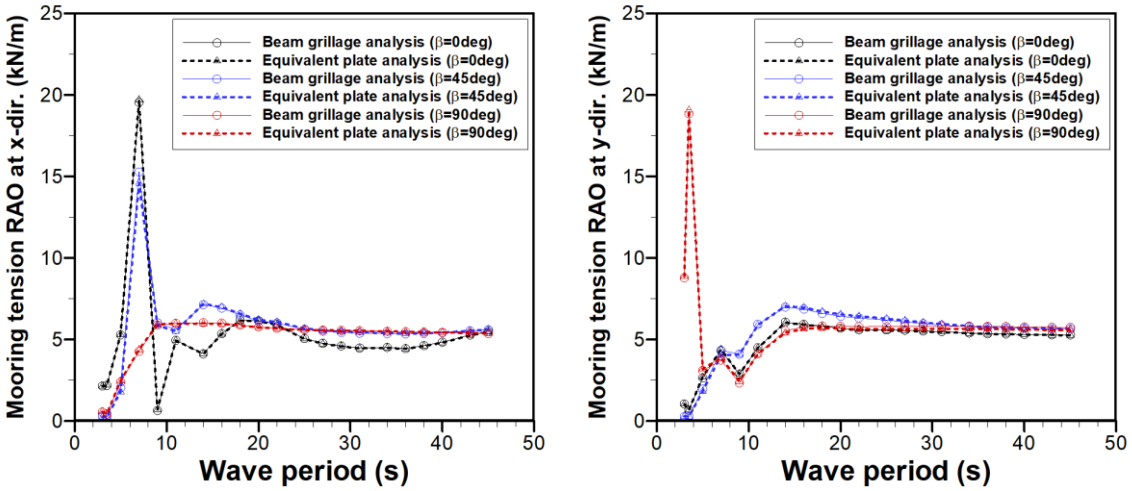

(a) Mooring tension RAO at longitudinal direction (b) Mooring tension RAO at lateral direction

Fig. 13 Mooring line tension RAO of example structure in regular waves

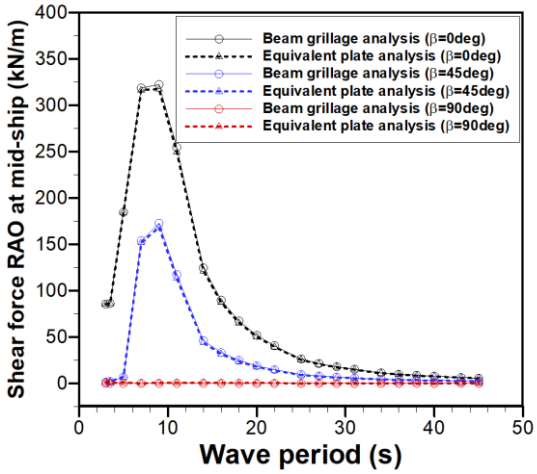

Fig. 14 Shear force RAO at mid-ship section of example structure in regular waves

Table 7 compares modeling efficiency, number of meshes, CPU time, etc. between beam grillage analysis and equivalent plate analysis. The equivalent plate method assumes a simple plate instead of complicated beam grillage. So, the key advantage is to reduce efforts in FEM modeling because the geometry is easier and simpler than the original beam grillage structure. Simpler modeling can reduce number of nodes or elements and it saves computing time as shown in Table 7. It could be said that the equivalent plate method can reduce number of meshes because its modeling is simpler and, although the modeling is simpler, its bending or tension accuracy is similar to complex beam grillage method. The advantage and limitation of the equivalent plate method are summarized in Table 8.

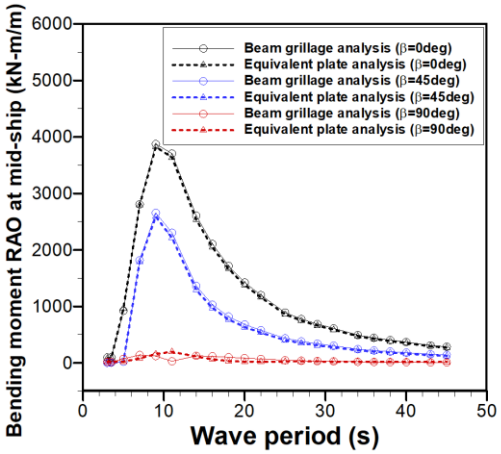

Fig. 15 Bending moment RAO at mid-ship section of example structure in regular waves

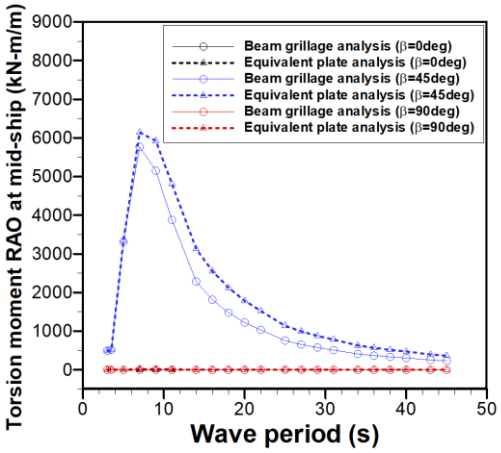

Fig. 16 Torsion moment RAO at mid-ship section of example structure in regular waves

Table 4 Peak values for Avg of example structure in irregular waves

Item	Avg		
	Beam grillage analysis	Equivalent plate analysis	Error
Surge at edge	0.061 m	0.062 m	1.64%
Sway at edge	0.055 m	0.055 m	0.00%
Heave at edge	0.440 m	0.442 m	0.45%
Surge at center	0.062 m	0.062 m	0.00%
Sway at center	0.055 m	0.055 m	0.00%
Heave at center	0.255 m	0.255 m	0.00%
Mooring line tension at *x*-dir.	3.439 kN	3.462 kN	0.67%
Mooring line tension at *y*-dir.	2.388 kN	2.413 kN	1.05%
Shear force at mid-ship section	277.079 kN	273.825 kN	-1.17%
Bending moment at mid-ship section	3041.152 kN-m	2999.891 kN-m	-1.36%
Torsion moment at mid-ship section	4590.120 kN-m	5153.159 kN-m	12.27%

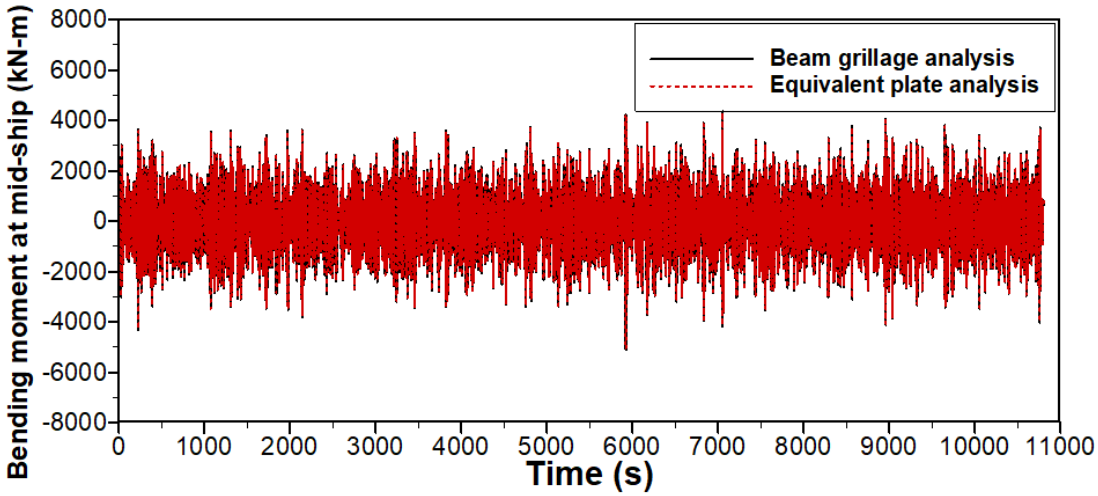

Fig. 17 Time series of bending moment at mid-ship section of example structure in irregular waves (H_s=1.5 m, T_p=9 s, heading angle=0 deg)

Table 5 Peak values for Max of example structure in irregular waves

Item	Max		
	Beam grillage analysis	Equivalent plate analysis	Error
Surge at edge	0.167 m	0.167 m	0.00%
Sway at edge	0.197 m	0.197 m	0.00%
Heave at edge	1.489 m	1.503 m	0.94%
Surge at center	0.167 m	0.167 m	0.00%
Sway at center	0.199 m	0.197 m	-1.01%
Heave at center	0.812 m	0.812 m	0.00%
Mooring line tension at *x*-dir.	9.660 kN	9.720 kN	0.62%
Mooring line tension at *y*-dir.	8.016 kN	8.061 kN	0.56%
Shear force at mid-ship section	458.563 kN	453.261 kN	-1.16%
Bending moment at mid-ship section	5114.328 kN-m	5066.770 kN-m	-0.93%
Torsion moment at mid-ship section	8073.246 kN-m	8992.259 kN-m	11.38%

Table 6 Responses of example structure in wind or current

Item	Wind induced responses			Current induced responses		
	Beam grillage analysis	Equivalent plate analysis	Error	Beam grillage analysis	Equivalent plate analysis	Error
Lateral displacement at edge	0.984 m	0.984 m	0.00%	0.041 m	0.041 m	0.00%
Lateral displacement at center	0.985 m	0.984 m	-0.10%	0.041 m	0.041 m	0.00%
Mooring line tension	47.932 kN	47.931 kN	0.00%	2.017 kN	2.017 kN	0.00%

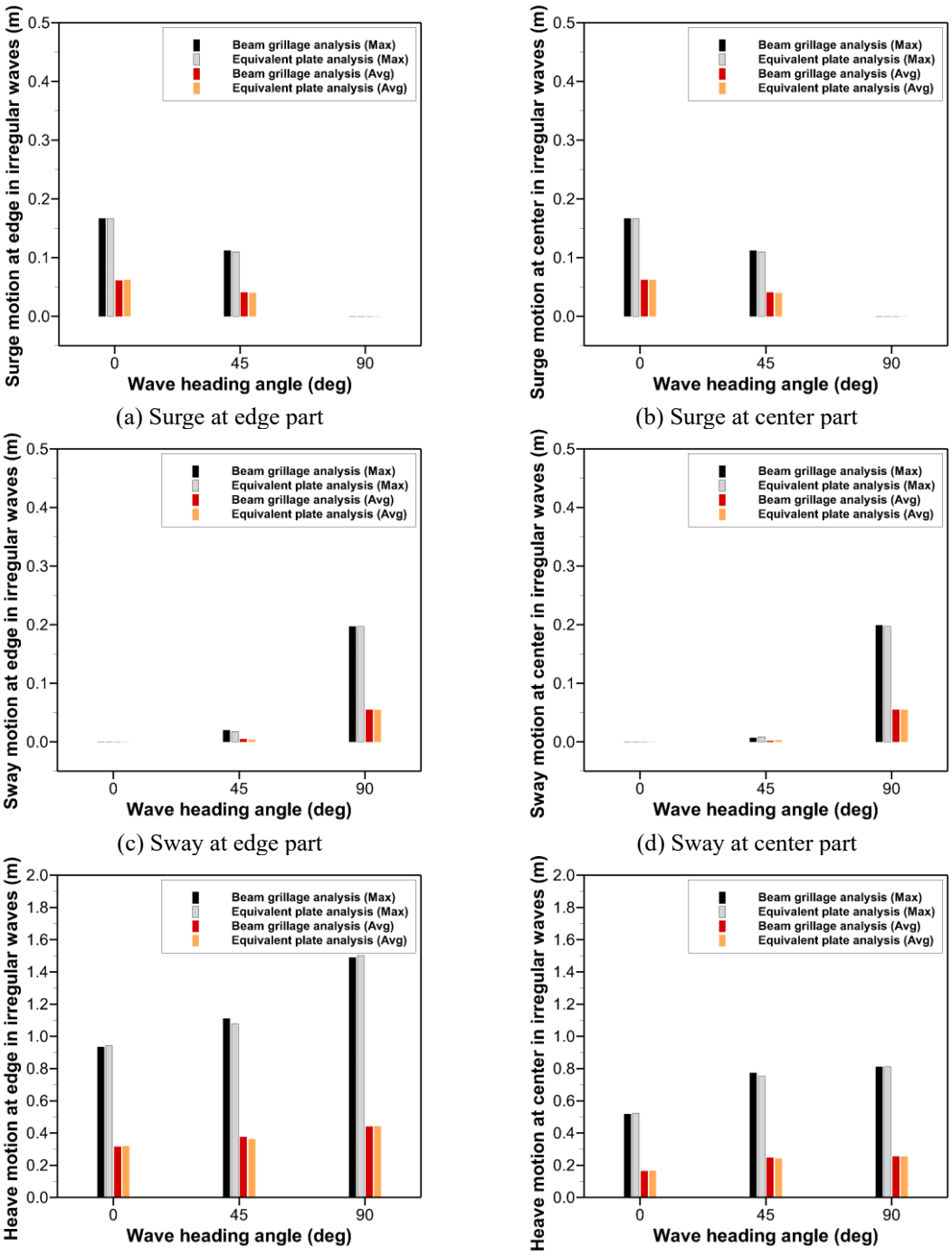

(a) Surge at edge part (b) Surge at center part

(c) Sway at edge part (d) Sway at center part

(e) Heave at edge part (f) Heave at center part

Fig. 18 *Max* and *Avg* motion of example structure in irregular waves (H_s=1.5 m, T_p=9 s)

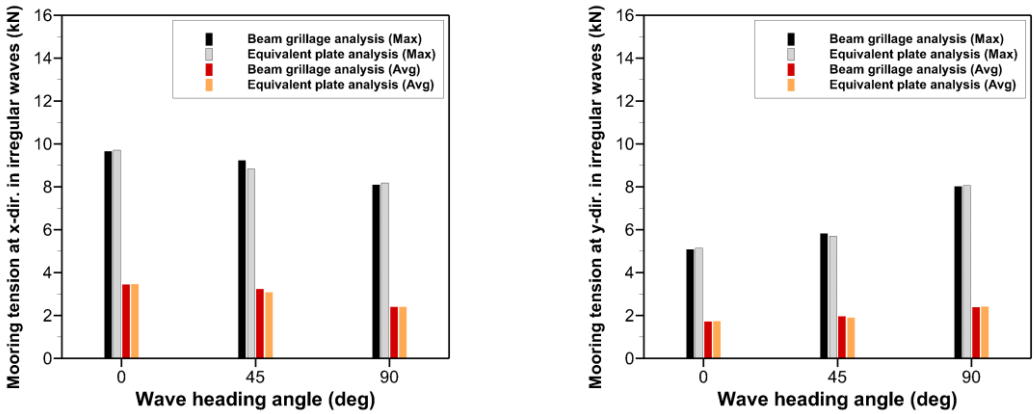

(a) Mooring tension at longitudinal direction (b) Mooring tension at lateral direction

Fig. 19 *Max* and *Avg* of mooring line tension of example structure in irregular waves (H_s=1.5 m, T_p=9 s)

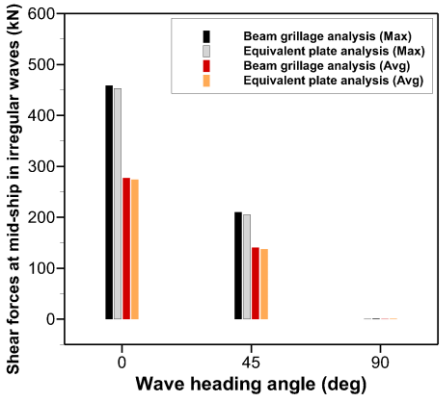

Fig. 20 *Max* and *Avg* of shear force at mid-ship section of example structure in irregular waves (H_s=1.5 m, T_p=9 s)

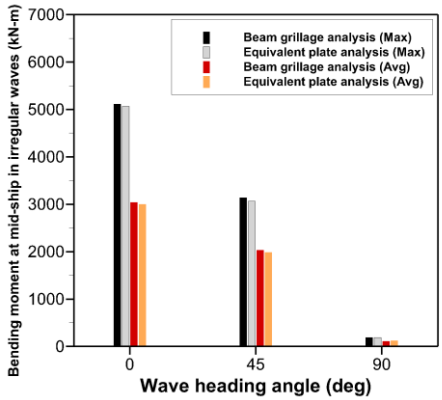

Fig. 21 *Max* and *Avg* of bending moment at mid-ship section of example structure in irregular waves (H_s=1.5 m, T_p=9 s)

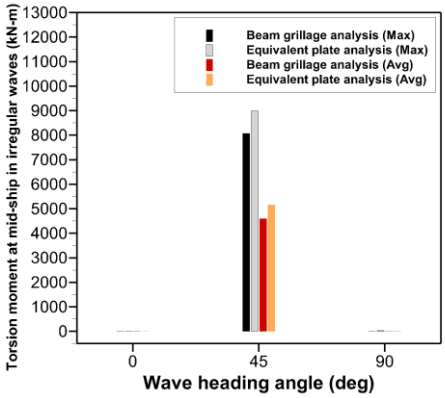

Fig. 22 *Max* and *Avg* of torsion moment at mid-ship section of example structure in irregular waves (H_s=1.5 m, T_p=9 s)

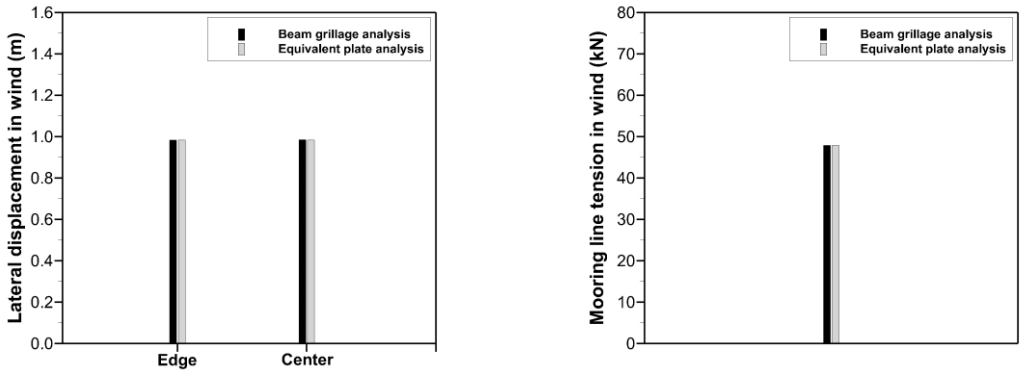

(a) Lateral displacements of platform (b) Mooring line tensions

Fig. 23 Responses of example structure in wind (wind speed=55 m/s)

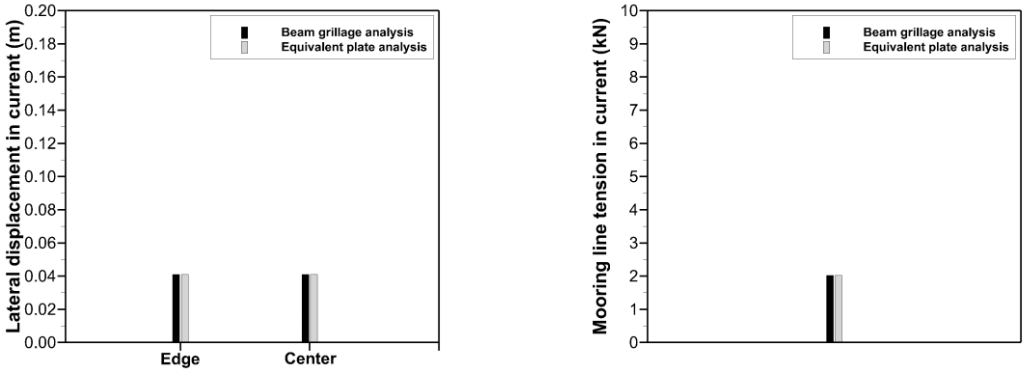

(a) Lateral displacements of platform (b) Mooring line tensions

Fig. 24 Responses of example structure in current (current speed=0.319 m/s)

Table 7 Comparison of modeling and computing efficiency

Item		Beam grillage analysis	Equivalent plate analysis
FEM modeling		Complicated	Easier & simpler
Number of nodes		8700	6051
Number of elements		11200	6904
CPU time	Analysis in regular wave	343.7656 sec	280.2031 sec
	Analysis in irregular wave	21454.98 sec	20416.33 sec
	Analysis in wind	1.563 sec	1.094 sec
	Analysis in current	1.594 sec	1.125 sec

Table 8 Summary of advantage and limitation of the equivalent plate method

Advantages	Limitations
• FEM modeling is easier and simpler. • Less CPU time than beam grillage method without losing motion, bending, shear and tension accuracy	• Simultaneous matching for bending & torsion is not easy. • Torsion accuracy is lower than bending accuracy.

5. Conclusions

This paper proposed an equivalent plate method to simply analyze multi-body floating structure connected with many beams. The method assumes complicated beam grillage structure to be a simple plate by introducing equivalent bending thickness and equivalent distributed mass. A multi-body floating solar platform with 400 floating bodies, 200 mooring lines and 100 connector beams was analyzed as a numerical example. Hydrodynamic forces, damping and added mass of floating bodies were formulate by HOBEM and beam or shell elements were formulated by FEM. Mode shapes, natural frequencies, RAO in regular waves and average & maximum responses in irregular waves of the example structure were calculated and their results were compared for the original beam grillage analysis and the equivalent plate analysis. Wind or current induced responses were also compared. Conclusions are derived from the numerical results.

(1) Mode shapes and natural frequencies by equivalent plate analysis are similar to those of beam grillage analysis. Errors of natural frequencies are less than 1% for surge, sway and bending modes. Error in torsional natural frequency is bigger and it is about 2%.

(2) In regular waves, RAO's of body motions, mooring line tensions, sectional shear forces and bending moments by equivalent plate analysis agree well to those by beam grillage analysis. Some errors are shown in RAO of sectional torsion moments.

(3) In irregular waves, average & maximum responses of body motions, mooring line tensions, sectional shear forces and bending moments by equivalent plate analysis agree well to those by beam grillage analysis. Their errors are less than 2% for peak values. In sectional torsion moments, the errors are bigger and they are 11~12%.

(4) In winds or currents, lateral displacements of the platform and mooring line tensions by equivalent plate analysis were nearly equal to those by beam grillage analysis.

(5) FEM modeling by equivalent plate analysis is easier and simpler than beam grillage analysis.

Number of nodes, number of elements and CPU time were reduced.

(6) The main purpose of this study is to show that the proposed scheme can reduce computation and modeling of complex beam grillage structure without losing bending accuracy by introducing equivalent bending thickness and mass. However, torsion errors are inevitable because simultaneous matching for bending & torsion stiffness or mass & rotational mass is not easy. So, some corrections are needed to match both. For example, torsional spring or rotational mass at every nodal points to compensate torsion errors without changing bending properties may be a specific solution. And, the future study is required to realize the method.

Acknowledgements

This research is a part of "Multipurpose Coastal Floating Infrastructure Technology" from the Korea Agency for Infrastructure Technology Advancement (KAIA) grant funded by the Ministry of Land, Infrastructure and Transport (Grant RS-2023-00250727/KRISO Grant PNS5250).

References

Abbasnia, A., Karimirad, M., Friel, D. and Whittaker, T. (2022), "Fully nonlinear dynamics of floating solar platform with twin hull by tubular floaters in ocean waves", *Ocean Eng.*, **257**, 111320. https://doi.org/10.1016/j.oceaneng.2022.111320.

Allman, D.J. (1988), "A quadrilateral finite element including vertex rotations for plane elasticity analysis", *Int. J. Numer. Method. Eng.*, **26**, 717-730. https://doi.org/10.1002/nme.1620260314.

Bathe, K.J. and Wilson, E.L. (1972), "Large eigenvalue problems in dynamic analysis", *ASCE J. Eng. Mech.*, **98**(6), 1471-1485. https://doi.org/10.1061/JMCEA3.0001693.

Choi, Y.R., Hong, S.Y. and Choi, H.S. (2001), "An analysis of second-order wave forces on floating bodies by using a higher-order boundary element method", *Ocean Eng.*, **28**, 117-138. https://doi.org/10.1016/S0029-8018(99)00064-5.

Chung, J. and Hulbert, G.M. (1993), "A time integration algorithm for structural dynamics with improved numerical dissipation: The generalized α-method", *J. Appl. Mech.*, **60**, 371-375. https://doi.org/10.1115/1.2900803.

Donea, J. and Lamain, L.G. (1987), "A modified representation of transverse shear in C0 quadrilateral plate elements", *Comput. Method. Appl. M.*, **63**(2), 183-207. https://doi.org/10.1016/0045-7825(87)90171-X.

Garrett, D.L. (2005), "Coupled analysis of floating production systems", *Ocean Eng.*, **32**(7), 802-816. https://doi.org/10.1016/j.oceaneng.2004.10.010.

Hong, S.Y., Kim, J.H., Cho, S.K., Choi, Y.R. and Kim, Y.S. (2005), "Numerical and experimental study on hydrodynamic interaction of side-by-side moored multiple vessels", *Ocean Eng.*, **32**(7), 783-801. https://doi.org/10.1016/j.oceaneng.2004.10.003.

Hong, S.Y., Kim, B.W. and Kim, H.S. (2018), "A hydroelastic analysis of beam-connected multi-body floating structure for solar power plant in waves", *Proceedings of the 13th World Congress on Computational Mechanics (WCCM XIII)*.

Jiang, Z., Dai, J., Saettone, S., Tora, G., He, Z., Bashir, M. and Souto-Iglesias, A. (2023), "Design and model test of a soft-connected lattice-structured floating solar photovoltaic concept for harsh offshore conditions", *Mar. Struct.*, **90**, 103426. https://doi.org/10.1016/j.marstruc.2023.103426.

Jin, C., Lee, I., Bakti, F., Kim, S. and Kim, M. (2025). "Multi-body-based 2D hydro-elasticity simulations in time domain for moored floating structure", *Eng. Struct.*, **329**, 119789. https://doi.org/10.1016/j.engstruct.2025.119789.

Kim, B.W., Cho, S.W., Kim, C.H. and Lee, I.W. (2005), "Determination of natural frequencies and mode

shapes of structures using subspace iteration method with accelerated starting vectors", *ASCE J. Struct. Eng.*, **131**(7), 1146-1149. https://doi.org/10.1061/(ASCE)0733-9445(2005)131:7(1146).

Kim, B.W. and Lee, K. (2024), "Hydro-dynamic behavior of multi-body floating solar platform with beam or shell connectors and comparison of design capacity", *Proceedings of the 34th International Ocean and Polar Engineering Conference (ISOPE 2024)*.

Kim, B.W., Sung, H.G., Kim, J.H. and Hong, S.Y. (2013), "Comparison of linear spring and nonlinear FEM methods in dynamic coupled analysis of floating structure and mooring system", *J. Fluid. Struct.*, **42**, 205-227. https://doi.org/10.1016/j.jfluidstructs.2013.07.002.

Kim, H.S. and Kim, B.W. (2019), "An efficient linearised dynamic analysis method for structural safety design of J-lay and S-lay pipeline installation", *Ships Offshore Struct.*, **14**(2), 204-219. https://doi.org/10.1080/17445302.2018.1493906.

Kim, H.S., Kim, B.W. and Hong, S.Y. (2020), "Comparative study on effect of buoys for floating sunlight generation system with numerous buoys and connection beams", *Int. J. Offshore Polar Eng.*, **30**(2), 209-219. https://doi.org/10.17736/ijope.2020.mk65.

Kim, H.S., Kim, B.W., Won, Y., Oh, Y.J., Lee, J., Hong, S.Y., Kang, K., Lee, S.K. and Park, J.J. (2021), "Experimental study on structural responses of floating photovoltaic system with numerous buoys and connection beams", *MTS/IEEE Oceans21*.

Kim, M.H., Ran, Z., Zheng, W., Bhat, S. and Beynet, P. (1999), "Hull/Mooring coupled dynamic analysis of a truss spar in time-domain", *Proceedings of the Ninth International Offshore and Polar Engineering Conference (ISOPE 1999)*.

Korea Ministry of Oceans and Fisheries (2017), *Harbor and Fishing Port Design Criteria Commentary-Design Condition*, KDS 64 10 10.

KRISO (2020~2024), *Core Technology Development of Hydro-elasticity Based Structural Damage Assessment for Offshore Structures considering Uncertainty*, KRISO R&D Project.

Newmark, N.M. (1959), "A method of computation for structural dynamics", *ASCE J. Eng. Mech.*, **85**(3), 67-94. https://doi.org/10.1061/JMCEA3.0000098.

Song, J., Kim, J., Chung, W.C., Jung, D. and Kang, Y.J. (2023), "Wave-induced structural response analysis of the supporting frames for multiconnected offshore floating photovoltaic units installed in the inner harbor", *Ocean Eng.*, **271**, 113812. https://doi.org/10.1016/j.oceaneng.2023.113812.

Xu, P. and Wellens, P.R. (2022), "Theoretical analysis of nonlinear fluid–structure interaction between large-scale polymer offshore floating photovoltaics and waves", *Ocean Eng.*, **249**, 110829. https://doi.org/10.1016/j.oceaneng.2022.110829.

Zheng, X.Y., Zheng, H.D., Lei, Y. and Chen, H. (2021), "Nonlinear stochastic responses of a newly developed floating wind-solar-aquaculture system", *Ocean Eng.*, **241**, 110055. https://doi.org/10.1016/j.oceaneng.2021.110055.

MK